Comparative study of the effect of fuel deoxygenation and polar species removal on jet fuel surface deposition

Alborzi, Ehsan; Gadsby, Phil; Ismail, Mohammed S.; Sheikhansari, Abdolkarim; Dwyer, Matthew. R.; Meijer, Anthony J. H. M.; Blakey, Simon G.; Pourkashanian, Mohamed

DOI:
10.1021/acs.energyfuels.8b03468

Comparative Study of the Effect of Fuel Deoxygenation and Polar Species Removal on Jet Fuel Surface Deposition

Ehsan Alborzi,*,† Phil Gadsby,† Mohammed S. Ismail,† Abdolkarim Sheikhansari,† Matthew. R. Dwyer,† Anthony J. H. M. Meijer,‡ Simon G. Blakey,¶ and Mohamed Pourkashanian†

†*Department of Mechanical Engineering, The University of Sheffield, Sheffield S3 7HF,UK*

‡*Department of Chemistry, The University of Sheffield, Sheffield, Sheffield S3 7HF,UK*

¶*Department of Mechanical Engineering, The University of Birmingham, Birmingham B15 2TT,UK*

E-mail: e.alborzi@sheffield.ac.uk

Abstract

The effect of near-complete deoxygenation and polar species removal on deposition propensity of a Jet A-1 fuel type, with marginal thermal oxidative stability was studied in a laboratory scale approach. The fuel deoxygenation was carried out via nitrogen purging and two types of bespoke zeolites were used separately in a packed bed reactor for partial polar separation. The treated fuel samples were assessed individually for deposition propensity, using "High Reynolds Thermal Stability(HiReTS)" test device. It was found that when the concentration of hydroperoxides in fuel is relatively high, polar removal is more effective way than the fuel deoxygenation in reducing carbonaceous deposits.

Furthermore, competitive adsorption of dissolved O_2 with polar species was studied for a model fuel doped with a few polar species, as well as for the Jet A-1 with marginal thermal stability, in the packed bed reactor with zeolite 3.7Å. The polar species added to the model fuel share the same functional groups as those in Jet A-1 with a strong impact on fuel thermal degradation and surface deposition. These include hexanoic acids, heaxnol, hexanal, hexanone, phenyl amine (aniline), butylated hydroxytoluene(BHT), dibutyl disulfide and Fe naphthenate.

A one-dimensional model for calculation of dissolved O_2 adsorption in the packed bed reactor was built using COMSOL Multiphysics. The modelling results were in good agreement with the induction period prior to the beginning of the O_2 adsorption, as well as the different stages of O_2 uptake during the competitive adsorption between dissolved O_2 and polar species in the Jet A-1 fuel. The calculation showed a discrepancy with the experimental results beyond the second phase of O_2 adsorption. More theories, assumptions and physical sub-models are required to build a more robust predictive model.

A new chemical reaction pathway based on the self-reaction of hydroperoxides was proposed as part of "Basic Autoxidation Scheme(BAS)" to justify the relatively high deposition propensity of the marginal fuel after near-complete deoxygenation. The viability of this reaction pathway was supported by the quantum chemistry calculations.

Introduction

Overview of chemistry of fuel autoxidation

Gas turbine fuels are exposed to thermal stress en-route from the fuel tank, through the engine fuel supply system to the combustion chamber. The increasing temperature of fuel, as it passes through the engine fuel supply system, initiates a multitude of chemical reactions in bulk fuel.[1] This results in the formation of a number of soluble and insoluble complex

organic molecules which are composed of hydrocarbons, sulfur, nitrogen and oxygen.[2] These species ultimately contribute to the formation of carbonaceous deposits on the surface of the fuel system. These deposits can block filter screens or fuel nozzles, cause disruption to the flow of fuel, and result in breakdown in the operation of specific engine components.

Different chemical pathways contribute to the changes in chemical composition of a thermally stressed jet fuel. Each of these needs a temperature at which they will dominate the formation of deposits. Using analytical grade n-dodecane as a simplified model fuel, Reddy[3] reported three temperature regimes. These include the autoxidation dominant, which occurs at the temperatures up to 300 °C, and the pyrolytic degradation, which proceeds at the temperature regimes above 500 °C. There is also an intermediate region reported that falls between the autoxidation and pyrolytic regimes.

Aviation fuel typically contains approximately 70 ppm of dissolved O_2, when is in equilibrium with air at atmospheric pressure and at room temperature. The molecular O_2 initiates a multitude of chemical reactions known as autoxidation. The autoxidation of liquid hydrocarbons has been broadly studied for pure single component hydrocarbons, with the carbon atom numbers in the range of petroleum based jet fuel (C_{10}-C_{12}). The results of these studies indicate that the autoxidation reactions proceed through a free radical mechanism.[4–7] The initiation step of autoxidation is manifested by the formation of free alkyl radicals, as presented schematically in rxn1. It is hypothesised that the catalytic effect of metal constituents of the fuel wetted surface plays a significant role in the initiation of autoxidation.[5] Through the propagation stage, the free radicals can react with dissolved oxygen as shown in rxn2. Another typical reaction in the propagation stage, which is rate determining, is the abstraction of one hydrogen atom from the substrate by $RO_2\cdot$, generating a hydroperoxide and an alkyl radical in conformity with the rxn3.

$$\mathrm{RH} \longrightarrow \mathrm{R}\cdot \tag{1}$$

$$\mathrm{R}\cdot + \mathrm{O_2} \longrightarrow \mathrm{RO_2}\cdot \tag{2}$$

$$\mathrm{RO_2}\cdot + \mathrm{RH} \longrightarrow \mathrm{RO_2H} + \mathrm{R}\cdot \tag{3}$$

There is much experimental evidence indicating that trace polar species including phenolic species[8,9] , reactive sulfur species such as sulfides and disulfides[10,11] and nitrogen components[12–16] play a significant role in the overall rate of autoxidation and surface deposition. The intervention of antioxidants is through the H-atom abstraction reaction from peroxy radicals as illustrated in rxn4. This reaction proceeds faster than the rxn3 due to the lower activation energy. Therefore, jet fuels with high concentration of phenolic compounds tend to oxidise slowly. However, these species have a significant impact on the increase of deposition rate.[17]

Hydroperoxides are another influential class of chemical species which significantly affect the overall rate of autoxidation.[1] It is important to note that hydroperoxides are inevitably found in micro-molar concentration in Jet-A1 during the storage period.[18] This class of species is also considered as the primary products of fuel autoxidation. However, they are susceptible to be thermally and/or catalytically decomposed under thermal exposure, as shown schematically in rxn5. Thermal decomposition of hydroperoxides is integrated into the "Basic Autoxidation Scheme(BAS)" of liquid hydrocarbon fuels to account for the maintenance of propagation stage in the absence of dissolved oxygen.[19,20]

As shown in rxn5, hydroperoxides partly undergo thermal decomposition(homolitic fission). However, reactions catalysed by the intervention of complexes of dissolved metals such as Cu, Fe and Mn cause this class of reaction proceed with a faster rate.[18,21] It is known that due to the low polarity of hydrocarbons, metals are not directly soluble in aviation fuels. However, the trace of metals are identified in aviation fuel in association with naturally occurring organic ligands. It is hypothesised that the organic ligand species are most likely to be a mixture of naphthenic acids. Fuel contacts different metal components during production and supply chains, which results in binding with naphthenic acids in the fuel, forming fuel soluble metal naphthenates.[22]

Another chemical pathway for decomposition of hydroperoxides is through the non-radical reactions with reactive sulfurs as illustrated in rxn6 and rxn7.[11] It is reported that reactive sulfurs and products of phenolic species in association with indoles and/or carbazoles contribute to the surface deposition.[4,18] However the underlying theory of the physico-chemical interactions of these species is not well understood. With the exception of nitrogen compounds, the role of the most significant heteroatomic species in fuel autoxidative deposition process is illustrated schematically in figure 1.

$$\mathrm{AH} + \mathrm{RO_2}\cdot \longrightarrow \mathrm{RO_2H} + \mathrm{A}\cdot \tag{4}$$

$$\mathrm{ROOH} \longrightarrow \mathrm{RO}\cdot + .\,\mathrm{OH} \tag{5}$$

$$\mathrm{ROOH} + \mathrm{RSR} \longrightarrow \mathrm{ROH} + \mathrm{sulfoxide} \tag{6}$$

$$\mathrm{ROOH} + \mathrm{RSSR} \longrightarrow \mathrm{ROH} + \text{thiosulfinate} \tag{7}$$

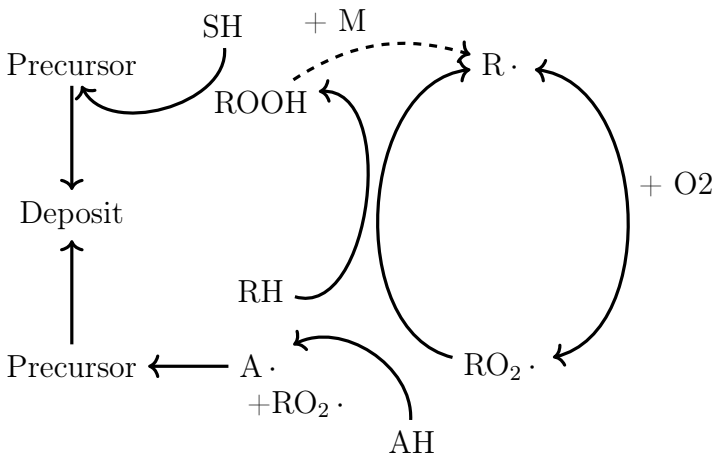

Figure 1: Autoxidation Scheme for liquid hydrocarbons along with pathways leading to deposit formation, adapted from[18]

Fuel cleansing through partial adsorptive separation of polar species and dissolved oxygen

Deoxygenation of aviation fuel via nitrogen purging has been widely used as a laboratory scale method for jet fuel thermal oxidative stability enhancement. In theory, this is achieved by prevention of peroxy radicals formation in rxn2. Membrane separation[23] is another method for aviation fuel deoxygenation by which a significant O_2 drop from 70 ppm to less than 1 ppm is reported. There is much experiential evidence to suggest that the positive impact of deoxygenation on surface deposition could be significantly different. This depends on the distribution of trace sulfur, nitrogen containing molecules and oxygenated species in the fuel.[10,12,24,25]

Attapulgus clay is widely used at refineries as part of wet treating processes and also is com-

monly utilised in places close to the airports in the US, to remove surface active components and other polar species. This is of great importance considering that aviation fuel is transported through multi-product supply chains and it may pick up trace of polars from previous delivery and distribution of other fuels.[26,27] Zeolite is another type of solid adsorbent used for aviation fuel deoxygenation with low efficacy in the lab scale applications.[28]

It is known that zeolites are highly porous crystalline aluminosilicates. Numerous zeolite species (with different chemical compositions, crystal structure and adsorption properties) are known. In general, zeolites are described as aluminosilicates with open 3-dimensional framework structures. They include corner-sharing TO_4 tetrahedra, where T is Si^{4+} and Al^{3+} which are loosely associated with framework oxygens O^{2-}. Each oxygen anion connects two cations and this yields a macro-molecular three dimensional framework with neutral SiO_2 and negatively charged $AlO_2{}^-$ tetrahedral building-blocks. The negative charge is compensated by additional non-framework cations such as Na^+ which is generally present after the synthesis of the zeolite. The crystalline structure of zeolite is honeycombed with relatively large cavities. Each cavity is connected through apertures or pores. The exact diameter of the pore depends on the coordination, type and the amount of cations and anions.[29,30]

Due to the presence of alumina, zeolites exhibit a negatively charged framework which is counter-balanced by positive cations. This results in a strong electrostatic field on the internal surface. Cations can be exchanged to calibrate the pore size or the adsorption characteristics. In theory, the ability to fine-tune the pores to determined uniform openings allows molecules smaller than the pore diameter to diffuse in whilst excluding the larger molecules, known as the confinement effect.[29] The molecular size discrimination by zeolites for branched hydrocarbons in comparison to the linear hydrocarbon molecules is reported in the literature.[31]

In addition to the selective adsorption by pore size, larger molecules can be adsorbed on the surface of pores of zeolites as a result of three major interactions: Van der Waals forces between zeolite pore walls and the adsorbate; electrostatic interactions between the adsorbate and Brönsted acid sites of zeolite; and the adsorbate-adsorbate interactions.[32] For instance, adsorption of alcohols in zeolites occurs through hydrogen bonding between the OH functional group with zeolite Brönsted acid sites. Furthermore, it is shown that with addition of carbon atom, the dispersion forces, which are the result of the interactions between the adsorbate and zeolite pore walls, become crucial factor in the adsorption affinity of the alcohols.[33]

In summary, the net effect of interactions between guest molecules and zeolites is controlled by the ratio of Si/Al.[34] Therefore, it is expected to observe a variety of chemisorption and physisorption of polar and non-polar species into the pores and surfaces of zeolites. For instance, studies using "Density Functional Theory(DFT)" demonstrated that zeolites exhibit both physisorption and chemisorption in binding with molecules such as CO_2, CO and H_2.[35–37] It is also reported that zeolites with smaller pore size show preferential adsorption between H_2, CH_4 and N_2 based on the molecular size. In contrast, it is shown that O_2 will bind with Al with the possibility of chemical interaction.[38] This is an important consideration when investigating the binding of autoxidation products with zeolites as not only structure and size will be dominant factors but the chemical composition of zeolites can play an important role.

One of the advantages of zeolites in the adsorption process is the sorbent regenerating characteristics. There are common methods for regeneration of zeolites which can be grouped into four types, used separately or in combination.[30] These include thermal swing, pressure swing, purge gas stripping and displacement cycle.

This study aims to compare the impact of near-complete fuel deoxygenation with partial polar species removal on propensity of surface carbonaceous deposits. This work is laboratory-scale; scaling-up for larger applications and higher level of technology readiness requires serious engineering considerations and was not part of this study.

Experimental Work

Baseline fuels and chemical composition

Three baseline fuels were used in this study: two types of Jet A-1 and a model fuel (i.e. a polar-free solvent composed of 5 normal paraffins in the range of C_{10} to C_{14}). The composition of major hydrocarbon constituents and the most significant deposition related to the polar species of the baseline fuels are shown in table1.

The Jet A-1 fuel samples were analysed for hydrocarbons, reactive sulfurs and antioxidants externally, using a test method developed by Intertek UK. This method identifies sulfur containing compounds and group types in the middle distillates using an Agilent 7890 N "Gas Chromatograph(GC)" equipped with a Zoex thermal modulation and an Agilent 355 sulfur chemiluminescence detector. Fuel acidity was also quantified by Intertek UK according to the ASTM D3242.

Quantification of sulfur classes was carried out via normalisation to the total sulfur content as determined by combustion followed by UV-Fluorescence. The $GC \times GC$ analysis separates sulfur-containing compounds based on their boiling points and polarity. Thus it was possible to elute the benzothiophenes and dibenzothiophenes in two well-defined bands, clearly separated from the band of thiophenes, sulfides and mercaptans. Hydrocarbon speciation was carried out using "UOP Method 990-11". This method determines the molecular type

homologous series based on the carbon number.

The polar nitrogen was quantified externally by "University of Dayton Research Institute (UDRI)", using multidimensional gas chromatography time of flight mass spectrometry, following the analytical method reported in the reference.[15] Dissolved metal analysis was performed in our lab using a calibrated Spectro-Ciros-Vision ICP-OES instrument. The total concentration of hydroperoxide in the baseline fuels were determined in our lab following the test method reported in the reference.[20]

Table 1: Composition of major hydrocarbon constituents along with sulfur, polar nitrogen, hydroperoxides and dissolved metals for the baseline fuels

		Baseline Fuel	
	Fuel sample A	Fuel sample B	Polar-free solvent
Chemical composition		**Concentration**	
n-Paraffins	20.67% m/m	19.56% m/m	97.2% m/m
iso-Paraffins	24.77% m/m	25.83% m/m	NA
cyclics	30.84% m/m	31.92% m/m	NA
Alkylbenzenes	16.18% m/m	15.12% m/m	1.1 %
Indans and tetralins	2.15% m/m	2.1% m/m	NA
Naphtalenes	1.33% m/m	1.28% m/m	NA
Antioxidant	25 mg/l	25 mg/l	NA
Acidity	0.08 $mgKOH/100g$	0.072 $mgKOH/100g$	NA
Thiols, Sulfides and Disulfides	835 mg/kg	812 mg/Kg	NA
Polar Nitrogen	12 mg/kg	12 mg/kg	NA
Total hydroperoxides	13.8 μM	4.1 μM	2.5 μM
Dissolved Fe	115 *ppb*	110 *ppb*	NA
Dissolved Cu	50 *ppb*	38 *ppb*	NA
Dissolved Zn	48 *ppb*	64 *ppb*	NA

Fuel thermal oxidative stability assessment

A HiReTS test device was used to assess the thermal stability of the baseline fuels and treated fuels for comparison. This test device is based on the ASTM D6811-02 test method. In this method, an aerated test fuel is filtered and pumped through an electrically heated capillary at turbulent regime. The capillary tube is controlled to maintain a constant fuel temperature of 290 °C at the tube exit.

The external surface of capillary is blackened to give a high thermal emissivity such that a

pyrometer can measure the real-time changes in the capillary wall temperature with the high degree of accuracy. Over time, the deposition of the carbonaceous materials on the inner surface of capillary tube causes an insulative effect. This results in localised areas of elevated external wall temperature. Our previous findings show that the profile of temperature rise along a heated tube in aero-engine representative condition is non-linear and fuel specific. The non-linear temperature rise along the external surface of a simulated burner feed arm under engine representative condition is reported in references.[39,40]

By virtue of mounting a pyrometer on an automated positioning bed, the temperature in the localised areas can be captured as discrete measurement points, along a small section of the capillary, and used to create a time-profile of temperature rise along the wall. The main advantage of the HiReTS method is the ability to quantify the thermal stability of fuel using relative measures such as HiReTS number. This number corresponds to the thickness of deposit inferred from the change to the thermal conduction between fuel and wetted wall. The calculation of the HiReTS number employs the difference between the final and minimum ΔT measurement in the data set generated at each of the twelve measurement positions. The total HiReTS number is calculated by summing this difference at each measurement position as shown in equation1. The test condition used in HiReTS is presented in table2.

Table 2: Test conditions in HiReTS

Test Parameters	**Values**
Flow Rate(ml/min)	35
Test temperature(°C)	290
Test Pressure(MPa)	2.0
Test Time(min)	120
Number of positions measured per scan(n)	12
Scans per test	25
Distance between measured position(mm)	2.5
Fuel aeration time(min)	12
Scan time(min)	5

$$\sum_{n=1}^{n=12} (\Delta T_{Final} - \Delta T_{min}) \tag{1}$$

Fuel deoxygenation and adsorptive fuel treatment

The effect of near-complete deoxygenation on deposition propensity of the baseline fuels was carried out using N_2 purging. Prior to the N_2 purging, the baseline fuels were aerated, as indicated in the ASTM D6811-02 test method. Level of fuel deoxygenation was monitored by an optical oxygen sensor which operates based on fluorescence quenching technology. The deoxygenated fuel samples were kept in sealed fuel drums to minimise the risk of ambient air diffusion and were instantly assessed for the surface deposition propensity in the HiReTS test device.

A packed bed reactor was used to explore the simultaneous effect of zeolites 3.7Å and 4.5Å on partial fuel deoxygenation and polar species removal. The packed bed reactor was a 1 m stainless steel tube with a 2.54 cm inner diameter and 6 K-type thermocouples inserted equally distant along the tube for temperature monitoring. The distance between two neighbouring thermocouples was 15 cm.

A "Proportional Integral Derivative (PID)"controller was used to heat the furnace up to a fixed set point temperature for each test. Once the furnace reached the set point temperature and settled, the tube reactor was filled up with sorbent and fuel and subsequently placed inside the furnace. If the tube was connected to the pump prior to the furnace warming up, the time required to fill the tube would have been longer. In this situation, adsorption capacity of solid adsorbent could have been changed due to the longer interaction with the fuel. Due to the absence of cooling effect, once the furnace reached the set point temperature, the time required for fuel inside the tube to reach to the set point is faster in comparison to the flowing system. This helps to reduce the effect of gradual temperature rise on the air solubility in fuel.[27]

The amount of zeolite was fixed in such away to fill up the isothermal region of the packed

bed reactor. Subsequently, a fixed low flow rate of 5 ml/min was set by means of a pump as a part of solvent delivery system in a "High Performance Liquid Chromatography(HPLC)". This was to create a long residence time for the adsorption process in the bed. The level of dissolved O_2 was monitored in-line by the optical oxygen sensor during each test. The position of the oxygen sensor was approximately 1 m downstream of the tube reactor. Since a standard complete HiReTS test requires 5 L of jet fuel(including test volume and rinsing), each test took approximately 17 h to obtain sufficient volume for thermal stability assessment in the HiReTS. It is important to note that three separate tests were carried out to find the temperature corresponding to the beginning of the adsorption. This was in the range of 25 to 75°C for both zeolites. Since dissolved O_2 was monitored in-line, the beginning of adsorption was based on O_2.

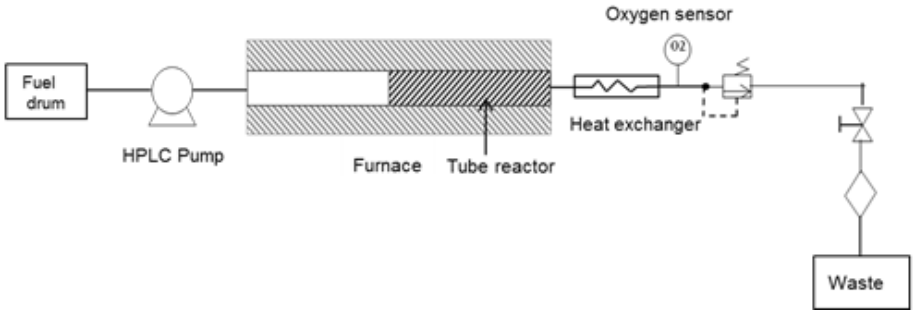

Figure 2: Schematic of packed bed reactor

To explore one by one interaction of the polar species with zeolites, the model fuel was doped with the known amount of polar species individually. This was followed by the adsorptive treatment using 10 ml cartridges, filled with 1 g sorbent. The cartridges were connected to a vacuum manifold so that a fixed flow rate of 1 drop/s was set for the treatment. The list of polar species and their concentrations in the model fuel is shown in table3. We deliberately added higher concentrations to the model fuel to minimise the quantification errors. It is worth to note that, although the selected polar species in this work share the same functional groups in their molecular structures with the polar species in a typical Jet A-1,

their molecular weight is significantly lower. Concentration of polar species in the treated samples were measured by gas chromatography with the exception of Fe naphthenate which was quantified by ICP-OES.

To explore the competitive adsorption between dissolved O_2 and polar species with zeolite, the model fuel doped with the polar species was treated with zeolite 3.7Å in the packed bed reactor. The amount of dissolved O_2 in the treated fuel samples was measured in-line by the optical oxygen sensor. The same measurement techniques as above were used for quantification of polar species. In the next stage, the marginal fuel was treated with 3.7Å in the packed bed reactor under the same test condition used for the model fuel for comparison. The reason for the use of zeolite 3.7Å rather than 4.5Å in the packed bed reactor was merely the availability of the raw materiel(chabazite) for the preparation of the coated pellets by the sorbent producer.

Table 3: List of polar species and concentration in model fuel

Polar species	**Supplier**	**Concentration**
Hexanoic acid(analytical grade)	Sigma-Aldrich	200 ppm
Hexanol(analytical grade)	Sigma-Aldrich	200 ppm
Hexanal(analytical grade)	Sigma-Aldrich	200 ppm
Hexanone(analytical grade)	Sigma-Aldrich	200 ppm
Cumene hydroperoxides(analytical grade)	Sigma-Aldrich	200 ppm
Dibutyl disulfide(analytical grade)	Sigma-Aldrich	200 ppm
Phenylamine(aniline)(analytical grade)	Sigma-Aldrich	200 ppm
Butylated hydroxytoluene(BHT)(analytical grade)	Sigma-Aldrich	200 ppm
0.012-0.015 mM Fe naphthenate(12% wt)	Fisher Scientific	200 ppb

Numerical Work

Packed bed reactor modelling

Two main approaches for simulation of diffusion in zeolites can be used including microscopic and macroscopic methods. In the microscopic approach, the kinetic properties of guest molecules are explicitly considered in modelling. However, in the macroscopic approach,

the zeolite is viewed as a continuous medium and kinetic properties of guest molecules are neglected. The macroscopic approach is advantageous as it can be used as a fast correlative model; the microscopic model is computationally expensive as it incorporates a variety of assumptions regarding individual particle motion, the interaction between the guest molecule and its host and interaction between the molecules themselves. Due to the complexity of jet fuel chemical composition, we used a macroscopic model assuming that the jet fuel is a binary mixture of a substrate and dissolved O_2 with the concentration of 70 ppm.

We assumed that the change of kinetics of O_2 adsorption over time is an indication for the competitive adsorption of other classes of species. Accordingly, a time-dependent, one dimensional model was created to calculate the adsorptive behaviour of dissolved O_2 in jet fuel via passing through a bed of zeolite 3.7Å. It was also assumed that the concentration of O_2 present in the mixture is small compared to the bulk fluid. Taking this into consideration, the transport of diluted species in porous media interface in COMSOL Multiphysics with convection and adsorption sub models was used. The convective/diffusive equations used in the interface is shown in the equation2.

$$\frac{\partial c_i}{\partial t} + \nabla.(-D.\nabla.c_i) + \mathbf{u}.\nabla.c_i = R_i \tag{2}$$

Where c_i represents the concentration of component i in mol/cm^3, D_i denotes the diffusion coefficient in m^2/s and R_i represents an expression for reaction rate of species i in $mol/m^3.s$ and $\mathbf{u}$ indicates the bulk average velocity of the fluid phase in m/s.

The first term on the left side of the equation accounts for the consumption (or accumulation) of the species i. The second term corresponds to the diffusive transport with respect to the interaction between the dilute species and the solvent. The third term on the left hand side of the equation illustrates the convective transport due to the average bulk velocity $\mathbf{u}$. The reaction source term on the right-hand side of mass balance equation accounts for a

chemical reaction or desorption of species i on a porous matrix.

The diffusive transport is solved in conformity with the Fick's law and the effective diffusion in porous medium was calculated according to the equation3. Freundlich model was used to solve the the adsorption of O_2 into the porous media.

$$D_e = \frac{\epsilon_p}{\tau_F} D_L \tag{3}$$

Where D_L represents the single phase diffusion coefficient for the species diluted in pure liquid phase in m^2/s, and τ_F accounts for the turtosity factor(dimensionless) and ϵ_p represents the porosity of medium. The transport of diluted species interface in COMSOL provides predefined expressions to calculate the turtosity factor in porous media according to the Millington and Quirk model.

The initial conditions and parameters used in the modelling are shown in table4.

Table 4: Initial conditions and parameters used in the modelling

Tube reactor inner diameter	0.0254 m
Tube reactor length	1 m
Packed bed length	0.5 m
Concentration of dissolved oxygen in jet fuel	1.8E-3 mol/l
Concentration of bulk fuel	4.7 mol/l
Fuel flow rate	5 ml/min
Zeolite porosity	0.47
Diffusion coefficient of molecular oxygen	5E-6m^2/s
Diffusion coefficient of bulk fuel	1E-7m^2/s
Freundlich constant for oxygen	1.8
Freundlich exponent for oxygen	6

The diffusion of molecules in a pore is classified in different regimes depending on the pore diameter. Accordingly, for macro-pores, which are of the order of 1 μm or larger, collisions between the adsorbing molecules occur much more frequently than collisions with the adsorbent and the wall. As a result, molecular diffusion becomes the dominant mechanism. The number of collisions of adsorbing molecules with the wall increases as the size of pores

decreases until it eventually becomes smaller than the mean free path of the molecules. At this point, Knudsen adsorption dominates and the molecular motion begins to be a function of pore size. For example, in the range of 20Å , when the pore diameter becomes comparable to the size of the adsorbing molecules, the ongoing molecules-wall interactions occur. Diffusion in the micro pores of zeolites usually occurs in this regime which is known as configurational diffusion. Under this regime of diffusion, the molecular motion is strongly affected by the exact size and shape of the zeolites' channels, the shape of the diffusing molecules, the interactions between the surface atoms and the diffusing molecules, temperature and concentration of the adsorbing molecules. As a consequence, it is quite challenging to derive generalised equations where all these aspects are included in diffusion coefficients for the systems. The values of diffusion coefficients in this case vary in a broad range from 10^{-8} to $10^{-20} \mathrm{m}^2\,\mathrm{s}^{-1}$. The readers are referred to the reference[41] for further information.

Quantum chemistry

Density Functional Theory (DFT) geometry optimisation and frequency calculations were carried out in the Gaussian 09 program at the UB3LYP/cc-pVTZ/IEF-PCM (Heptane) level of theory.[42–48] All structures were calculated using the singlet wave functions with the HOMO and LUMO mixed to break the symmetry of the system and allow them to be open shell singlet species.

The geometries of reactants, products and transitions states of the peroxides reactions were all calculated. The reactants and products were considered optimised if the frequency calculation had no imaginary frequencies. The transition states were considered optimised if they had a single imaginary frequency along the reaction coordinate of interest. The optimised structure for all of the calculations can be found in the supporting information. The Arrhenius parameters were obtained from the DFT calculations using the thermodynamic

parameters from the frequency calculations.[49]

From the equations below,23 the Arrhenius equation can be linked to the enthalpy and entropy of the reactions. The activation energy(Ea) was taken as the enthalpy change between the reactants and the transition states, and pre-exponential factor(A) was obtained from the entropic term.

The rate of a chemical reaction can be given from by the Arrhenius equation, where A is pre-exponential collision factor and Ea is the activation energy as shown in equation4.

$$k = A\ exp(\frac{-Ea}{RT}) \tag{4}$$

The rate constant can also be written as illustrated in 5, where the pre-exponential factor has been split up into a temperature dependent component and an entropic component.

$$k = \frac{KbT}{h} exp(\frac{\Delta S}{R})\ exp(\frac{-Ea}{RT}) \tag{5}$$

In a solvent, the activation energy can be substituted for the enthalpy of activation as presented in equation6.

$$k = \frac{KbT}{h} exp(\frac{\Delta S}{R})\ exp(\frac{-\Delta H}{RT}) \tag{6}$$

This indicates that the Arrhenius pre-exponential factor can be calculated using equation7.

$$A = \frac{KbT}{h} exp(\frac{\Delta S}{R}) \tag{7}$$

Results and Discussion

Effect of deoxygenation on surface deposition propensity of baseline fuels

Given surface deposition propensity of the baseline fuels, hereafter fuel sample A is referred to as marginal fuel and fuel sample B as stable fuel respectively. The impact of near-complete deoxygenation on deposition propensity of baseline fuels is shown in figure3a. This effect on marginal fuel results in a noticeable reduction in deposition propensity. Nevertheless, the high value of the HiReTS number demonstrates that deoxygenated marginal fuel is still highly thermally unstable.

It can be observed that the impact of near-completed deoxygenation on deposition propensity of stable fuel is positive; however, this fuel was already very thermally stable to show a significant enhancement in surface deposition tendency. The model fuel was highly thermally stable due to the absence of polar species. Due to the drastic response of marginal fuel to the change of surface deposition propensity with near-complete deoxygenation, this fuel was used for further investigation in this work.

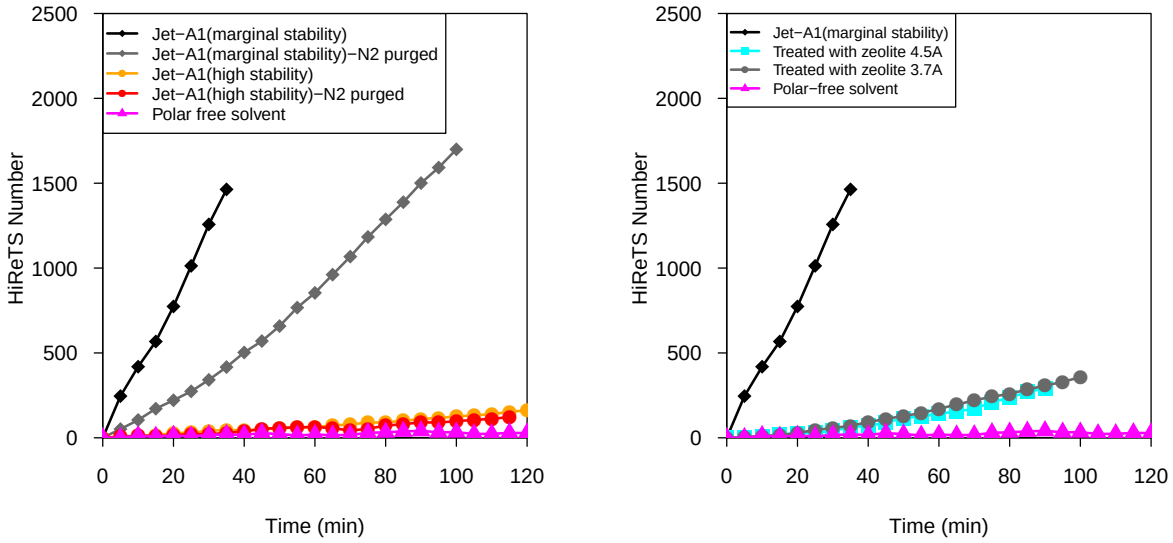

(a) Effect of near-complete deoxygenation on deposition

(b) Effect of polar species removal on deposition

Figure 3: a) Effect of near-complete deoxygenation via N_2 purging on deposition propensity of baseline fuels, b) Effect of polar species removal on deposition propensity of marginal fuel

In conformity with the kinetics of autoxidation in BAS[7] , in the presence of O_2 in bulk fuel, rxn2 requires no activation energy and it therefore proceeds very fast. Subsequently, $RO_2\cdot$ reacts slowly with RH generating RO_2H and $R\cdot$. The literature data for the activation energy required for this reaction are in the range of 10-18 $\mathrm{kcal\,mol^{-1}}$.[7,18] A related point to consider is that the generated $RO_2\cdot$ can react with the radicals originating from phenolic antioxidant, as illustrated schematically in figure1. This reaction is one of the possible ways that leads to the formation of precursor molecules for the generation of surface deposits.

In theory, when fuel is deoxygenated, rxn2 cannot proceed; therefore the formation of $RO_2\cdot$ via routine autoxidation pathways is interrupted. Hypothetically, this should disrupt the propagation stage and consequently the formation of deposit precursor, linked to the reaction of $RO_2\cdot$, and radical of phenolic antioxidant is prevented. However, it was observed that, despite near-complete deoxygenation, marginal fuel exhibits a high deposition propensity. In

addition, despite substantial enhancement in surface deposition propensity of marginal fuel via treatment with zeolites, the treated fuel showed an increasing deposition tendency over time in the HiReTS test device.

To explain these behaviours, chemical analysis of the post-treated samples as well as the results of individual interaction of the limited number of polar species with zeolites were used as discussed below.

Comparison of one by one interaction of selected polar species with zeolites

The results of one by one interaction of polar species with zeolites are presented in figure4. The percentage of removal shown in the figure is defined in conformity with the equation 8.

$$\%\ removal = \frac{amount\ of\ polar\ in\ treated\ sample}{amount\ of\ polar\ in\ model\ fuel\ doped\ with\ polar\ prior\ to\ the\ treatment} \times 100 \quad (8)$$

It can be observed that the highest percentage of removal corresponds to the oxygenated species with a decreasing trend from hexanoic acid to hexanal. The trend continues to decline steadily from hexanal to aniline and BHT, followed by a substantial drop to dibutyl disulfide. The overall trend of percentage of adsorption is the same for both zeolites; however, zeolite 4.7Å presents slightly higher adsorption. This is likely to be attributed to the bigger pore size, given that the ratio of Si/Al was the same for both zeolites.

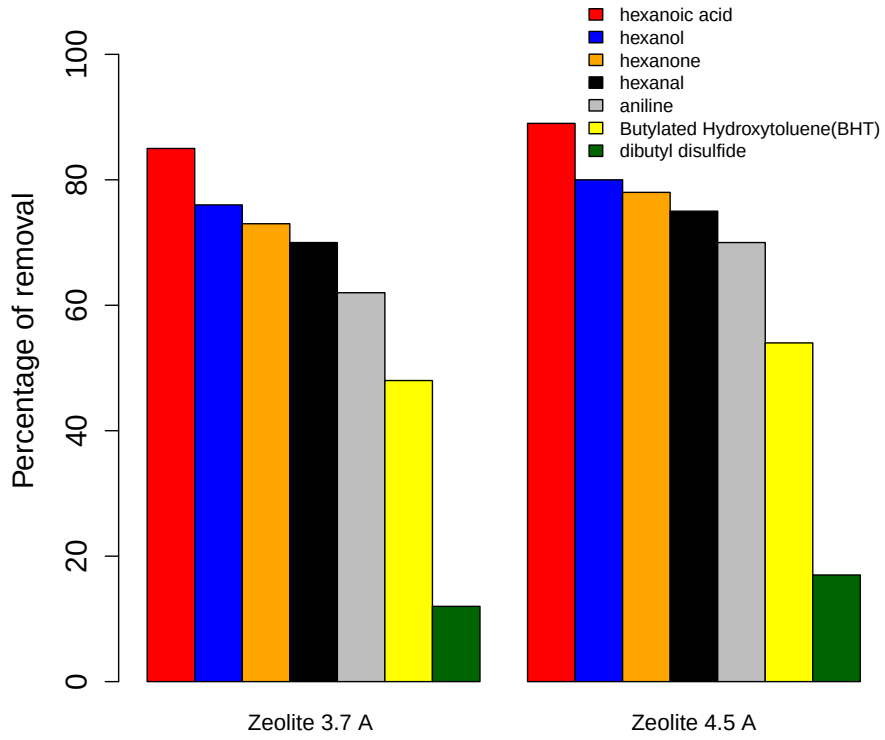

Figure 4: One by one adsorption of polar species by zeolites 3.7Å and 4.5Å

The investigation of the intermolecular interactions of polar species in zeolites requires extensive molecular modelling work which is currently under way. Alternatively, we used "Hansen Solubility Parameter(HSP)"[50] as a simplistic approach to interpret the results presented in the figure4. HSP is defined in terms of three parameters for each molecule, including dispersion(δ_D), dipole moment(δ_P) and hydrogen bonding(δ_D), as shown in equation9.[50]

$$\delta^2 = \delta D^2 + \delta P^2 + \delta H^2 \tag{9}$$

Table5 presents the estimated solubility parameters for the selected polar species, using HSPiP 5^{th} Edition 5.1.04 software.[51] The HSP values were used to present three dimensional

vectors corresponding to the model fuel and the polar species in a spatial region known as the Hansen space. Geometrical presentation of this space is not presented here due to the complexity for the interpretation. Instead, the distance between two vectors in this space can be used as the likelihood of intermolecular interactions between two species in such away that the closer they are, the more solubility(interactions) they have. We calculated the distance of the polar species from the model fuel in conformity with the equation10; see figure5.

$$Ra^2 = 4(\delta D1 - \delta D2)^2 + (\delta P1 - \delta P2)^2 + (\delta H1 - \delta H2)^2 \tag{10}$$

The results shown in the figure5 indicate that the molecular interactions between the model fuel and the oxygenated polars, as well as aniline, is relatively lower than BHT and dibutyl disulfide . Given that the hydrogen bonding term for the oxygenated species and aniline is higher, it is expected to observe that these species show the higher percentage of removal by zeolites than BHT and dibutyl disulfide.

Contrary to the higher molecular interactions of BHT with the model fuel, the percentage of removal of this species by zeolites indicates a high adsorption propensity. This is likely to be attributed to the role of π-electrons of aromatic ring in forming hydrogen bonding with the Brönsted acid sites of zeolite as reported in the reference.[52]

The lowest percentage of removal of dibutyl disulfide by zeolites is likely to be attributed to the low electrostatic interactions of this species with the Brönsted acid sites of the zeolites. In addition, the branched molecular structure of dibutyl disulfide might be a preventing factor for diffusion through the pores. The results of adsorption of cumene hydroperoxide and Fe naphthenate were not conclusive, hence are not presented in this article.

One of the limitations of HSP values is the uncertainties for the dipole moment parameter

and hydrogen bonding term for some species.[53] For instance, the estimated value of the hydrogen bonding term for hexanoic acid is incorrectly lower than heaxnol. It is important to note that the O−H group in carboxylic acids is more strongly polarised than the O−H group of alcohols due to the presence of the adjacent carbonyl group(C=O). In fact, the dipole present in carboxylic acids allows these spices to participate in hydrogen bonding, behaving as both H-bond donor and acceptor. Such a high tendency of carboxylic acids for hydrogen bonding is a strong justification for the highest percentage of removal of hexanoic acid when compared to the other polar species.

Table 5: Hansen Solubility Parameters for the model fuel and polar species

	Hansen Solubility Parameters		
Chemical species	**Dispersion**($MP^{0.5}$)	**Dipole moment**($MP^{0.5}$)	**Hydrogen bonding**($MP^{0.5}$)
Model fuel(n-dodecane)	16.2	0	0
Hexanoic acid	16.3	4.2	12.2
1-Hexanol	15.9	5.8	12.5
1-Hexanal	15.8	8.4	5.3
1-Hexanone	17.2	6.2	7.6
Aniline	19.4	5.1	10.2
BHT	16.5	0.9	4.5
Dibutyl disulfide	16.4	4.1	2.6

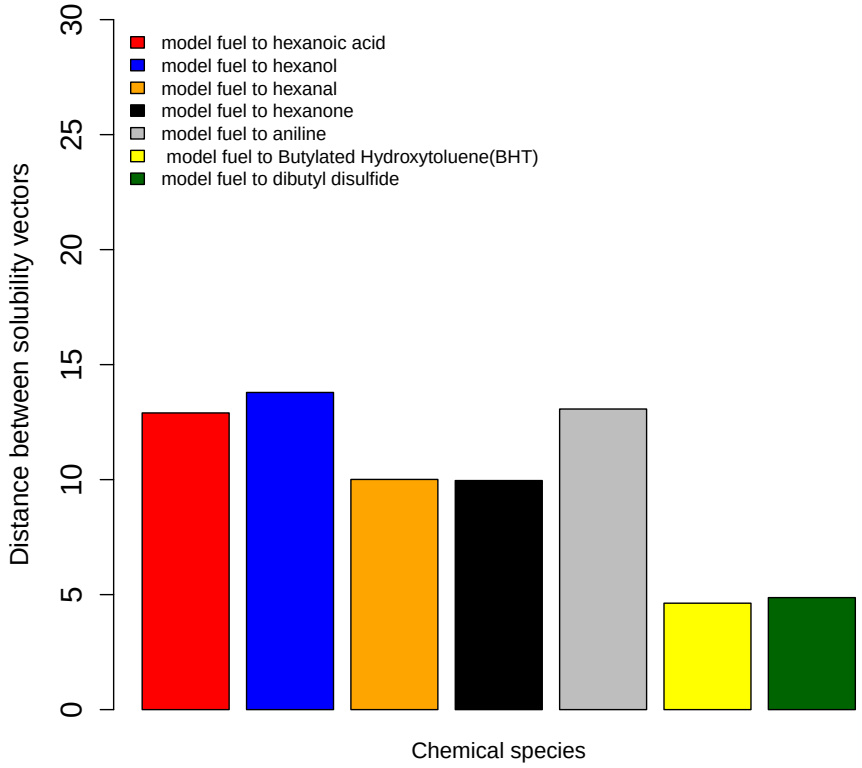

Figure 5: Distance between vectors of the model fuel and polar species

Investigation of competitive adsorption between O_2 and polars on zeolite 3.7Å in the packed bed reactor

The result of O_2 adsorption onto zeolite 3.7Å bed from model fuel doped with the polar species, carried out in the packed bed reactor, is shown in figure6a.

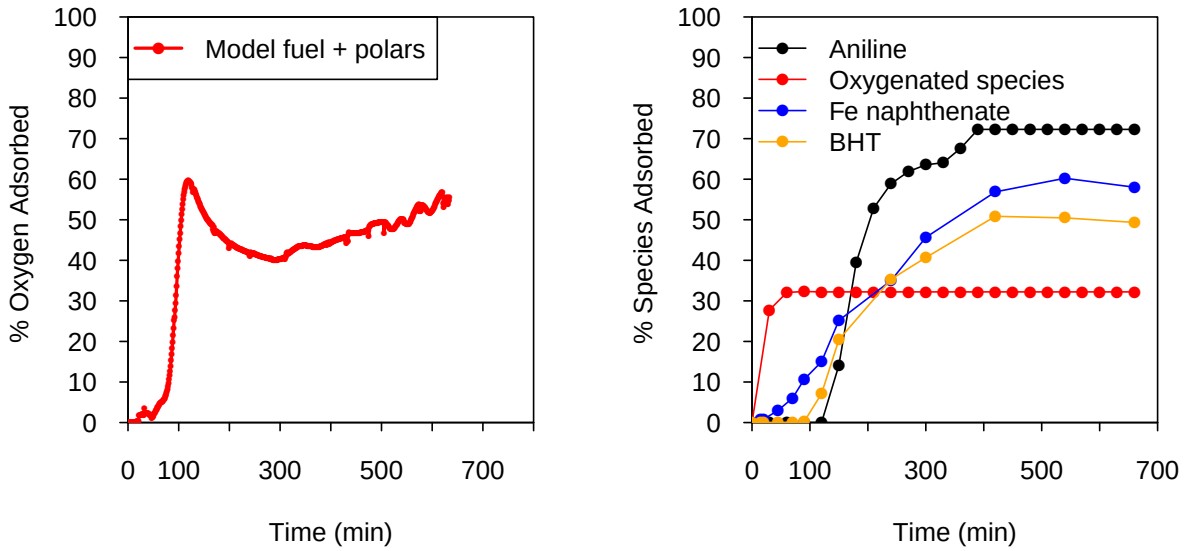

(a) Adsorption of O_2

(b) Adsorption of polars

Figure 6: a) Multi stage adsorption of O_2 from model fuel doped with the polar species, b) Adsorption of polar species from model fuel doped with the polar species, the samples for polar separation were taken through a valve, 2 m downstream of the packed bed

The results indicate that the O_2 adsorption begins approximately after 60-70 min of the test. This is followed by 60% increase over a period of 50-60 min, and an immediate decrease for the next 120 min. The reduction of O_2 adsorption is relatively sharp at the beginning and decelerates gradually for the next 180 min. A turning point, to which we refer as the beginning of the second phase of O_2 adsorption, occurred at approximately 300 min of the test time. During this phase, O_2 adsorption increased linearly.

The change in O_2 adsorption over time is likely to be attributed to a complex competitive adsorption between polar species and dissolved O_2 as supported by the results shown in figure6b. It can be observed that the oxygenated groups such as alcohol, aldehyde, ketone and acids collectively adsorbed by the zeolite 3.7Å within the first 60 min of the experiment. Fe naphthenate showed a slower adsorption rate in comparison to the oxygenated species. However, the results indicate that uptake capacity of zeolite 3.7Å for Fe naphthenate is mod-

erately higher than the oxygenated species. It is likely that the first delay in O_2 adsorption shown in figure6a is linked to the fast kinetics of the oxygenated species and Fe naphthenate in zeolite 3.7Å.

Adsorption of BHT and aniline started at approximately same time (with BHT slightly earlier). This time corresponds to the reduction of O_2 adsorption, as shown in figure6a. The adsorption of BHT, Fe naphthenate and aniline reached a plateau after approximately 350 min of the test. This point matches with the beginning of the second phase of O_2 adsorption. The results of adsorption of cumene hydroperoxide and dibutyl disulfide were not conclusive and therefore were not presented here.

The results shown in the figure7a indicate that the adsorption of O_2 from marginal fuel, followed the same trend as the model fuel doped with polar species with different timing. It can be seen that O_2 adsorption started moderately after approximately 30 min but decreased substantially over time. Subsequently, O_2 adsorption increased gradually in a linear trend over the next 350 min. Such a long delay prior to the substantial O_2 adsorption is likely to be attributed to the lower concentration of polar species in the marginal fuel. That is to say, the time required for bed saturation for the case of model fuel doped with higher concentration of polar species is shorter than the real fuel containing lower concentrations of polar species.

A sudden increase in O_2 adsorption was observed after approximately 450 min with a maximum of 60% reached in about 50-60 min. The maximum level achieved is identical to the case of the model fuel doped with the polar species. After this point, O_2 adsorption decreased with the same trend as the model fuel. However, a longer test for the marginal fuel is required to observe if the second phase of O_2 can take place. The results of figure7b indicate that the adsorption of Fe-bonded species and BHT from the marginal fuel followed

the same trend as model fuel doped with polar species; however, the time needed to reach to plateau for these polars are different for marginal and model fuels.

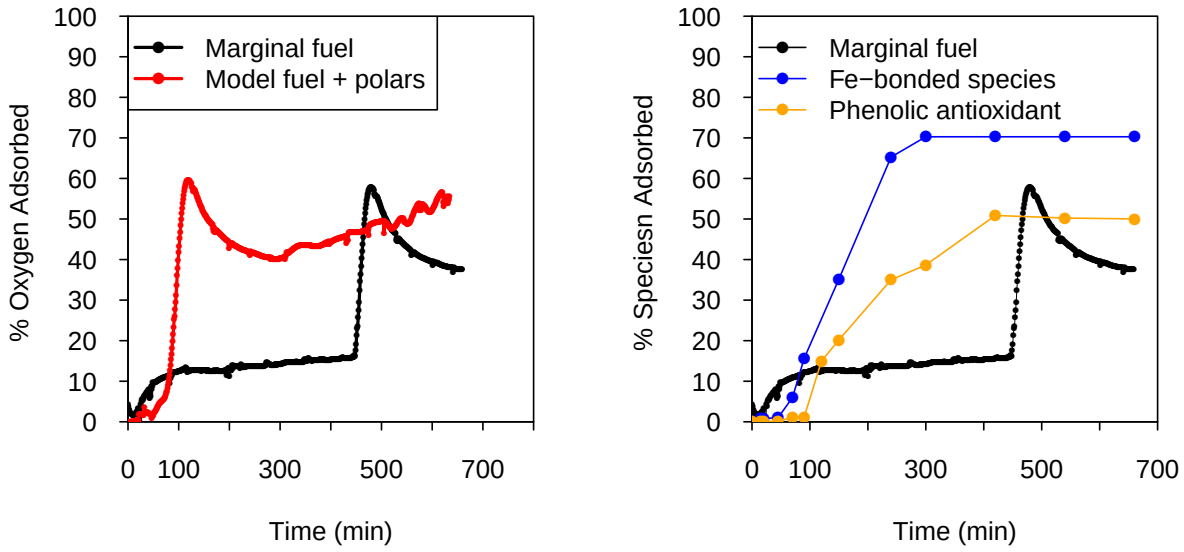

(a) O_2 adsorption from marginal and model fuel

(b) Adsorption of phenolic antioxidants and Fe-bonded species from marginal fuel

Figure 7: a) Comparison of multi stage O_2 adsorption from marginal and model fuel, b) Fe-bonded and phenolic antioxidant adsorption from marginal fuelthe samples for polar separation were taken through a valve, 2 m downstream of the packed bed

Role of hydroperoxides in near-complete fuel deoxygenated condition

Given the results of Fe-bonded and phenolic adsorption by zeolite 3.7Å and combining these to the relatively high concentration of hydroperoxides in the marginal fuel as shown in table2, we proposed an additional chemical pathway to the BAS, known as self-reaction of hydroperoxides. We used quantum chemistry to determine the kinetic parameters of this chemical pathway to interpret the results shown in figure3a and figure3b.

The self-reaction of hydroperoxides was first proposed by Bateman[54] and cited by Denisov,[7] as presented schematically in rxn7.

$$2\,\mathrm{ROOH} \longrightarrow \mathrm{RO}\cdot + \mathrm{H_2O} + \mathrm{RO_2}\cdot \tag{7}$$

As presented in figure 8, quantum chemistry calculations indicate that the self-reaction of hydroperoxides can proceed through a concerted and two-step route. These pathways are thermodynamically favourable and the radicals, formed during the first step of a two-step pathway, react with no barrier to form polar and non-radical products. Interestingly, one of which is another hydroperoxide species, therefore maintaining autoxidation cycle through their role in the propagation stage. We also noted that the transition state between the peroxyl and alkoxy radical fragments and the final products could not be located. This indicates that the self-reaction of hydroperoxides is barrierless or the energy barrier is very small. As such, the overall barrier to reaction is likely to stand as +33.6 kcal mol^{-1}.

A number of conclusions can be drawn from these calculations: the first conclusion is that an energy difference of +4.2 kcal mol^{-1}, between the two possible pathways, indicates that the reaction proceeds through the two step mechanism. The second conclusion that can be made from these calculations is that, even with a barrier of +33.6 kcal mol^{-1}, this pathway is a viable reaction in the thermally-stressed fuel, as it is approximately 10 kcal mol^{-1} lower than that for the thermal decomposition of hydroperoxides, with the same order for the pre-exponential factor of around 1x10^{15}(mol,L,s).[18,19,55]

It is important to note that the DFT calculations represent the upper value of the reaction barrier; however, due to the poor treatment of the electronic structure in this system, the barrier is likely over-estimated. This is also supported by the values presented in the literature[7,54] , although the exact methods used to determine those barriers are unknown. As

such, future work will be carried out using high level quantum chemistry theories to better understand this reaction.

In summary, given that the overriding difference between the two baseline fuels tested in this work was the concentration of hydroperoxides and considering the fact that the self-reaction of hydroperoxides is kinetically more probable than thermal decomposition, it is likely that the self-reaction of hydroperoxide is responsible for the increasing deposition tendency of the treated marginal fuel over the thermal exposure time in the HiReTS tube. It is important to note that the underlying chemistry of hydroperoxides and thier link to the surface deposition requires further research.

In the case of near-complete deoxygenation of marginal fuel, as illustrated in figure3a, the high propensity of fuel for deposit formation, is likely to be attributed to the catalytic decomposition of hydroperoxides, as this class of reactions requires approximately +10 kcal mol^{-1}.[18] This class of reactions is responsible for the formation of a series of chemical species, known as the secondary products of autoxidation. These include: alcohols, ketones, aldehydes and acids which collectively contribute to the formation of surface deposition through complex reactions with reactive sulfures, antioxidants and polar nitrogen.

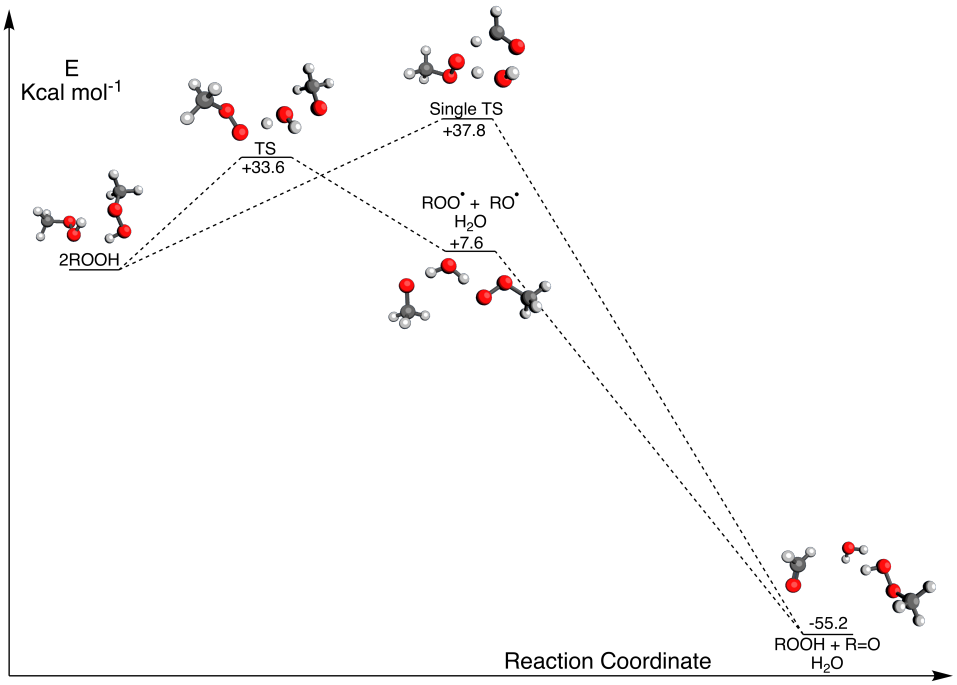

Figure 8: Calculated reaction surface of the self reaction of methyl peroxide. The calculations were performed at the UB3LYP/cc-pVTZ/PCM (heptane) level of theory. It is clear that the reaction proceeds through a two step mechanism, at the energy barrier difference of +4.2kcal mol^{-1} means +99% of the reaction goes through this pathway at expected temperatures.

Calculation of competitive adsorption in packed bed reactor

Simulation of simultaneous adsorption of various groups of polars and dissolved O_2 by the packed bed is interesting from the microscopic modelling point of view. However, as mentioned in the modelling section of this article, a number of assumptions and theories should be integrated into the microscopic modelling approach which collectively makes the simulation rather challenging and computationally expensive. These include the individual molecular motion, the physico-chemical interactions between zeolite pores and adsorbing molecules(polar species and molecular O_2), as well as the interactions amongst molecules during diffusion and adsorption. Understanding these interactions require an extensive quantum chemistry and molecular dynamics calculations along with experiments which is beyond the scope of this article. Therefore, for simplicity, in our macroscopic modelling approach,

all the molecular-level assumptions were ignored.

Initially, it was assumed that the dissolved oxygen separation in the packed bed reactor is purely based on the physisorption. For the physisorption, the only tuning parameters are the last two in table4, namely "Freundlich constant for oxygen" and "Freundlich exponent for oxygen ". These parameters can control the adsorption capacity and the induction period prior to the first phase of adsorption. For simplicity, to include the interference of chemical interactions during physisorption, all possible chemical interactions were treated as one phenomenological metamathematical expression, purely based on the experimental observations presented in figure 7, using the reaction source term in equation2.

The modelling results presented in the figure9a illustrate the adsorption of dissolved O_2 onto the bed of zeolite 3.7Å. The modelling results are in good agreement with the partial adsorption of dissolved O_2 from marginal fuel during the induction period and the first and second phases of adsorption. However, there is a discrepancy between the model results and the measurement data after the second phase of adsorption.

A closer look at the modelling results indicates that the beginning of adsorption process was predicted with a good degree of accuracy as shown in the figure9b. The beginning of adsorption process is manifested by an induction period which is likely to be attributed to the adsorption of the oxygenated species as observed in figure6b. This demonstrates that the model can be used for calculation of time needed for the beginning of adsorption of the oxygenated species. As the results of figure9b show, after $t = 50\ min$, the model results indicate a plateau while the measurements show a slow adsorption of dissolved O_2. However, this requires more in-depth understanding of physico-chemical interactions during this phase.

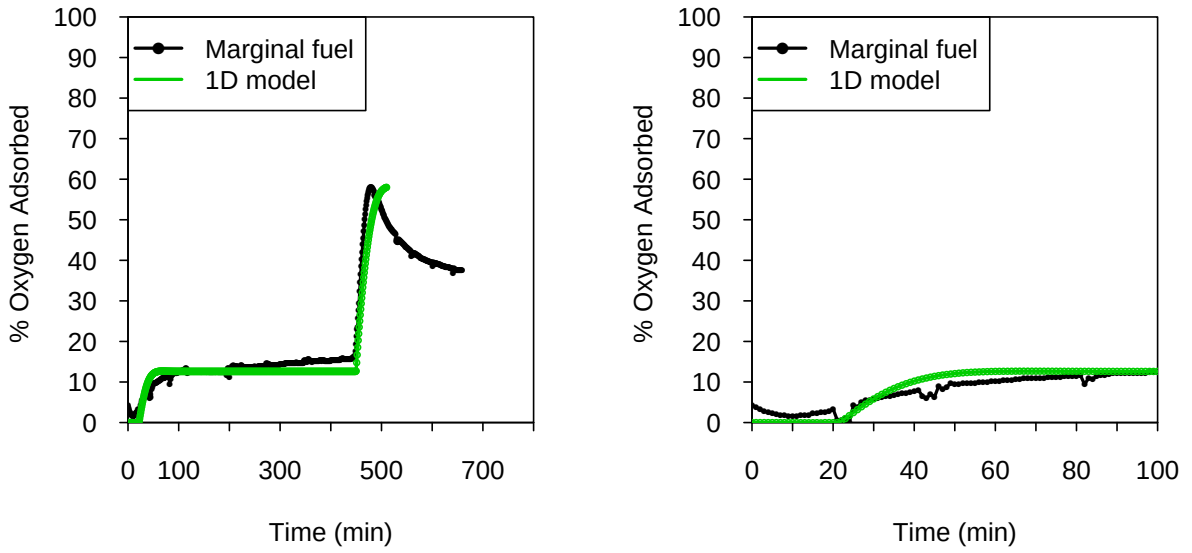

(a) Calculation of different stages of adsorption

(b) Calculation of induction period and first stage of adsorption

Figure 9: Prediction of different stages of O_2 during competitive adsorption from marginal through the packed bed

Conclusions

The sensitivity of deposition propensity of a fuel, with marginal thermal oxidative stability, to deoxygenation and polar species removal was studied. The deoxygenation was achieved by N_2 purging while polar species removal was carried out by the application of two types of bespoke adsorbents including zeolite 3.7Å and 4.5Å in a packed bed reactor.

Our experimental findings demonstrate that when the concentration of total hydroperoxides in jet fuel is relatively high, the fuel deoxygenation is not an effective way to reduce deposition propensity. This is likely to be attributed to the the self-reaction of hydroperoxides which results in generation of primary and secondary oxygenated products(hydroperoxides and spices with carbonyl groups) thus participating in prorogation stage of fuel autoxidation. Our quantum chemistry calculations indicate that self-reaction of hydroperoxides is a

thermodynamically viable two-step reaction.

The competitive adsorption of O_2 with some of the polar species by zeolite 3.7Å for a model fuel was studied. It was found that the beginning of O_2 adsorption is hindered by the fast adsorption of the oxygenated species. Moreover, when the oxygenated species reached a plateau, O_2 adsorption proceeded with fast kinetics. A maximum uptake capacity of approximately 60% was recorded for O_2 followed by a moderate decrease. It appears that the reduction in O_2 adsorption corresponds to the fast adsorption of aniline, and moderate adsorption of BHT and Fe naphthenate. Furthermore, the results showed that when the adsorption of these species reaches a plateau, O_2 begins to adsorb again with slower kinetics.

The similar trend for competitive O_2 adsorption by zeolite 3.7Å for marginal fuel was observed. However, it can be seen that the beginning of O_2 adsorption time is substantially longer than that in the model fuel doped with the polar species. This is likely to be attributed to the lower concentration of polar species in the marginal fuel in comparison with the model fuel. There is a similar trend for decrease of O_2 adsorption for marginal fuel after the maximum uptake capacity which resembles the competitive adsorption of Fe- bonded molecules and phenolic antioxidant.

The results of one dimensional model can be used to calculate the duration of hindrance for O_2 adsorption and the maximum uptake capacity of O_2. The time needed for the start of O_2adsorption can be used as an indication for the adsorption of oxygenated products. The model falls short of being applicable to calculate the second phase of competitive adsorption. Fundamental physical model is required to build an integrated model to predict the entire process.

Acknowledgement

This work was supported by the Horizon 2020-Clean Sky 2 programme under research grant agreement 145251. The authors would like to knowledge Dr.Nicolas Grosejan of Johnson Matthey for solid adsorbent preparation and Richard Striebich of UDRI for polar species analysis.

References

(1) Hazlett, R N, *Thermal Oxidation Stability of Aviation Turbine Fuels*; ASTM, 1991.

(2) Beaver, B.; Gao, L.; Burgess-Clifford, C.; Sobkowiak, M. On the Mechanisms of Formation of Thermal Oxidative Deposits in Jet Fuels. Are Unified Mechanisms Possible for Both Storage and Thermal Oxidative Deposit Formation for Middle Distillate Fuels? *Energy & Fuels* **2005**, *19*, 1574–1579.

(3) Reddy, K. T.; Cernansky, N. P.; Cohen, R. S. Modified reaction mechanism of aerated n-dodecane liquid flowing over heated metal tubes. *Energy & Fuels* **1988**, *2*, 205–213.

(4) Jones, E. G.; Balster, W. J. Phenomenological Study of the Formation of Insolubles in a Jet-A Fuel. *Energy & Fuels* **1993**, *7*, 968–977.

(5) Jones, E. G.; Balster, L. M.; Balster, W. J. Autoxidation of Aviation Fuels in Heated Tubes : Surface Effects. *Energy & Fuels* **1996**, *10*, 831–836.

(6) Kuprowicz, N. J.; Ervin, J. S.; Zabarnick, S. Modeling the liquid-phase oxidation of hydrocarbons over a range of temperatures and dissolved oxygen concentrations with pseudo-detailed chemical kinetics. *Fuel* **2004**, *83*, 1795–1801.

(7) Denisov, E. T.; Afanas'ev, I. B. *Oxidation and Antioxidants in Organic Chemistry and Biology*; CRC Press, 2005.

(8) Jones, E. G.; Balster, L. M. Impact of Additives on the Autoxidation of a Thermally Stable Aviation Fuel. *Energy & Fuels* **1997**, *11*, 610–614.

(9) Grinstead, B.; Zabarnick, S. Studies of Jet Fuel Thermal Stability, Oxidation, and Additives Using an Isothermal Oxidation Apparatus Equipped with an Oxygen Sensor. *Energy & Fuels* **1999**, *13*, 756–760.

(10) Taylor, W. F. Deposit Formation from Deoxygenated Hydrocarbons. II. Effect of Trace Sulfur Compounds. *Industrial & Engineering Chemistry Product Research and Development* **1976**, *15*, 64–68.

(11) Zabarnick, S.; Mick, M. S. Inhibition of Jet Fuel Oxidation by Addition of Hydroperoxide-Decomposing Species. *Industrial & Engineering Chemistry Research* **1999**, 3557–3563.

(12) Taylor, W. F.; Frankenfeld, J. W. Deposit Formation from Deoxygenated Hydrocarbons. 3. Effects of Trace Nitrogen and Oxygen Compounds. *Industrial & Engineering Chemistry Product Research and Development* **1978**, *17*, 86–90.

(13) Ervin, J. S.; Williams, T. F. Dissolved Oxygen Concentration and Jet Fuel Deposition. *Industrial & Engineering Chemistry Research* **1996**, *35*, 899–904.

(14) Balster, L. M.; Zabarnick, S.; Striebich, R. C.; Shafer, L. M.; West, Z. J. Analysis of Polar Species in Jet Fuel and Determination of Their Role in Autoxidative Deposit Formation. *Energy & Fuels* **2006**, *20*, 2564–2571.

(15) Striebich, R. C.; Contreras, J.; Balster, L. M.; West, Z.; Shafer, L. M.; Zabarnick, S. Identification of Polar Species in Aviation Fuels using Multidimensional Gas Chromatography-Time of Flight Mass Spectrometry. *Energy & Fuels* **2009**, *23*, 5474–5482.

(16) Commodo, M.; Fabris, I.; Groth, C. P. T.; Gülder, Ö. L. Analysis of Aviation Fuel Thermal Oxidative Stability by Electrospray Ionization Mass Spectrometry (ESI–MS). *Energy & Fuels* **2011**, *25*, 2142–2150.

(17) Taylor W F, *Development of High Stability Fuel, ESSO Research and Engineering Report*; 1972.

(18) Kuprowicz, N. J.; Zabarnick, S.; West, Z. J.; Ervin, J. S.; Edwards, T. Use of Measured Species Class Concentrations With Chemical Kinetic Modelling for the Prediction of Autoxidation and Deposition of Jet Fuels. *Energy & Fuels* **2007**, *21*, 530–544.

(19) Zabarnick, S. Chemical Kinetic Modeling of Jet Fuel Autoxidation and Antioxidant Chemistry. *Industrial & Engineering Chemistry Research* **1993**, *32*, 1012–1017.

(20) West, Z. J.; Zabarnick, S.; Striebich, R. C. Determination of Hydroperoxides in Jet Fuel via Reaction with Triphenylphosphine. *Industrial & Engineering Chemistry Research* **2005**, *44*, 3377–3383.

(21) Pickard, J. M.; Jones, E. G. Catalysis of Jet-A Fuel Autoxidation by Fe_2O_3. *Energy & Fuels* **1997**, *11*, 1232–1236.

(22) Zabarnick, S.; DeWitt, M. J.; Striebich, R. C.; Gunasekera, T. S.; Ervin, J.; Briones, A.; Shafer, L.; Fernando, S.; Graham, J.; West, Z.; Stouffer, S.; Vangsness, M.; Harruff-Miller, B. *Fuels and Combustion Technologies for Aerospace Propulsion*; 2016.

(23) Spadaccini, L.; Huang, H. On-Line Fuel Deoxygenation for Coke Suppression. *Journal of Engineering for Gas Turbines and Power* **2003**, *125*, 686–692.

(24) Taylor, W. F. Deposit Formation from Deoxygenated Hydrocarbons. I. General Features. *Industrial & Engineering Chemistry Product Research and Development* **1974**, *13*, 133–138.

(25) Frankenfeld, J. W.; Taylor, W. F. Deposit Formation from Deoxygenated Hydrocarbons. 4. Studies in Pure Compound Systems. *Industrial & Engineering Chemistry Product Research and Development* **1980**, *19*, 65–70.

(26) Naegeli, D, The Role of Sulfur in the Thermal Stability of Jet Fuel. ASME-GT. 1999.

(27) *Handbook of Aviation Fuel Properties*, 4th ed.; Coordinating Research Council, 2014.

(28) Darrah S, *Jet Fuel Deoxygenation, AFWAL-TR-88-2081 Interim Report,*; 1988.

(29) Van Bekkum, H.; Flanigen, E. M.; Jensen, J. C. *Introduction to Zeolite and Science Practice* ; Elsevier, 1991.

(30) Kulprathipanja, S. *Zeolites in Industrial Separation and Catalysis* ; Willey, 2010.

(31) Bendoraitis, J. G.; Chester, A. W.; Dwyer, F. G.; Garwood, W. E. Pore Size and Shape Effects in Zeolite Catalysis. *Studies in Surface Science and Catalysis* **1986**, *28*, 669–675.

(32) Mallon, E. E.; Bhan, A.; Tsapatsis, M. Driving Forces for Adsorption of Polyols onto Zeolites from Aqueous Solutions. *The Journal of Physical Chemistry B* **2010**, *114*, 1939–1945, PMID: 20070098.

(33) Nguyen, C. M.; Reyniers, M. F.; Marin, B. G. Theoretical study of the adsorption of C1-C4 primary alcohols in HZSM5. *Physical Chemistry Chemical Physics* **2010**, *12*, 9481–9493.

(34) Jha, B. and Singh, D N, *Basics of Zeolites. In: Fly Ash Zeolites. Advanced Structured Materials*; Elsevier Inc., 2016.

(35) Density functional theory study on the adsorption of H 2S and other claus process tail gas components on copper- and silver-exchanged Y zeolites. *Journal of Physical Chemistry C* **2012**, *116*, 3561–3575.

(36) Smith, D. G. A.; Patkowski, K. Benchmarking the CO2 Adsorption Energy on Carbon Nanotubes. *The Journal of Physical Chemistry C* **2015**, *119*, 4934–4948.

(37) Shang, J.; Li, G.; Webley, P. A.; Liu, J. Z. A density functional theory study for the adsorption of various gases on a caesium-exchanged trapdoor chabazite. *Computational Materials Science* **2016**, *122*, 307–313.

(38) Fischer, M.; Bell, R. G. Modeling CO2 Adsorption in Zeolites Using DFT-Derived Charges: Comparing System-Specific and Generic Models. *The Journal of Physical Chemistry C* **2013**, *117*, 24446–24454.

(39) Alborzi, E.; Blakey, S.; Ghadbeigi, H.; Pinna, C.; Lewis, C. Investigation of surface deposition in a simulated fuel injector feed arm with sudden expansion/contraction. *Fuel* **2016**, *186*, 534 – 543.

(40) Alborzi, E.; Blakey, S.; Ghadbeigi, H.; Pinna, C. Prediction of growth of jet fuel autoxidative deposits at inner surface of a replicated jet engine burner feed arm. *Fuel* **2018**, *214*, 528–537.

(41) Kärger, J. Measurement of Diffusion in Zeolites—A Never Ending Challenge? *Adsorption* **2003**, *9*, 29–35.

(42) Becke, A. D. Density-functional thermochemistry. III. The role of exact exchange. *The Journal of Chemical Physics* **1993**, *98*, 5648–5652.

(43) Dunning, T. H. Gaussian basis sets for use in correlated molecular calculations. I. The atoms boron through neon and hydrogen. *The Journal of Chemical Physics* **1989**, *90*, 1007–1023.

(44) Wilson, A. K.; van Mourik, T.; Dunning, T. H. Gaussian basis sets for use in correlated molecular calculations. VI. Sextuple zeta correlation consistent basis sets for boron through neon. *Journal of Molecular Structure: THEOCHEM* **1996**, *388*, 339–349.

(45) Kendall, R. A.; Dunning, T. H.; Harrison, R. J. Electron affinities of the first-row atoms revisited. Systematic basis sets and wave functions. *The Journal of Chemical Physics* **1992**, *96*, 6796–6806.

(46) Woon, D. E.; Dunning, T. H. Gaussian basis sets for use in correlated molecular calculations. III. The atoms aluminum through argon. *The Journal of Chemical Physics* **1993**, *98*, 1358–1371.

(47) Peterson, K. A.; Woon, D. E.; Dunning, T. H. Benchmark calculations with correlated molecular wave functions. IV. The classical barrier height of the H+H2=H2+H reaction. *The Journal of Chemical Physics* **1994**, *100*, 7410–7415.

(48) Tomasi, J.; Mennucci, B.; Cammi, R. Quantum mechanical continuum solvation models. *Chemical Reviews* **2005**, *105*, 2999–3093.

(49) Ochterski, J. W.; Ph, D. Thermochemistry in Gaussian. *Gaussian Inc Pittsburgh PA* **2000**, *264*, 1–19.

(50) M, H. C. *Hansen Solubility Parameters, A User's Handbook*, 2nd ed.; CRC Press, 2007.

(51) Abbot, S. HSP Basics. `https://www.stevenabbott.co.uk/practical-solubility/hsp-basics.php`.

(52) Javadian, S.; Ektefa, F. An efficient approach to explore the adsorption of benzene and phenol on nanostructured catalysts: a DFT analysis. *RSC Adv.* **2015**, *5*, 100799–100808.

(53) Stefanis, E.; Panayiotou, C. Prediction of Hansen Solubility Parameters with a New Group-Contribution Method. *International Journal of Thermophysics* **2008**, *29*, 568–585.

(54) Bateman, L.; Hughes, H.; Morris, A. Hydroperoxide decomposition in relation to the initiation of radical chain reactions. *Discuss. Faraday Soc.* **1953**, *14*, 190–199.

(55) Zabarnick, S. Pseudo-Detailed Chemical Kinetic Modeling of Antioxidant Chemistry for Jet Fuel Applications. *Energy & Fuels* **1998**, *0624*, 547–553.